Power Splitting Versus Time Switching Based Cooperative Relaying Protocols for SWIPT in NOMA Systems

Huu Q. Tran [1,2], Ca V. Phan[1], Quoc-Tuan Vien[3]

[1]*Ho Chi Minh City University of Technology and Education, Vietnam. E-mail: ttdv08@gmail.com/huutq.ncs@hcmute.edu.vn;capv@hcmute.edu.vn*
[2]*Industrial University of Ho Chi Minh City, Vietnam. E-mail: tranquyhuu@iuh.edu.vn*
[3]*Middlesex University, United Kingdom. E-mail: q.vien@mdx.ac.uk*

Abstract

Non-orthogonal multiple access (NOMA) along with wireless power transfer have recently been adapted to cooperative communications for 5G and beyond wireless networks. This paper investigates NOMA based cooperative relaying wireless-powered networks (CRWPNs) where, decode-and-forward (DF) relaying and successive interference cancellation are both employed at a wireless-powered intermediate node. For simultaneous wireless information and power transfer (SWIPT), power-splitting relaying (PSR) and time switching-based relaying (TSR) protocols are considered in the NOMA based CRWPN. As a result, the combination of cooperative relaying power domain NOMA network and PSR and TSR protocols is proposed in this paper. The outage performance and ergodic rate of both protocols are analysed for evaluation of the impacts of energy harvesting (EH) time, EH efficiency, power splitting ratio, source data rate, and the distance between the nodes. In addition, two delay limited transmission (DLT) and delay tolerant transmission (DTT) modes are considered in this network model to investigate the throughput and ergodic rate of the system according to the source transmission rate. It is shown that the cooperative relaying NOMA (CRNOMA) scheme achieves a lower outage probability when compared to the conventional orthogonal multiple access (OMA) schemes. Additionally, the PSR outperforms the TSR in both low and high signal-to-noise ratio (*SNR*) regions in terms of throughput, ergodic rate and energy efficiency. For instance, the outage probability of CRNOMA for both PSR and TSR in *SNR* range of from -10 dB to +20 dB (i.e. a low *SNR* region) decreases gradually but not linearly. However, in *SNR*

range of from +20 dB to +40 dB (i.e. a high *SNR* region), the outage probability of CRNOMA for both PSR and TSR decreases quickly. Furthermore, the energy efficiency is shown to be considerably enhanced with the employment of EH for CRNOMA. Finally, the impacts of the distance between the nodes on the performance and a comparison between two scenarios of having and without having direct links are evaluated.

Keywords:
Non-orthogonal multiple access (NOMA), energy harvesting (EH), information processing (IP), radio-frequency (RF), power-splitting relaying (PSR), time switching-based relaying (TSR), decode-and-forward (DF).

---

1. Introduction

With the rapid development of wireless communication technologies as well as demands of tremendously enhanced mobile communication performance, the technologies being used in 4G have shown their limits, which paves the way for the development of 5G [1]-[4]. These demands include simultaneous data transfer, high speed, massive connectivity, low latency and high spectral efficiency, etc.

As one of techniques evolved in the 5G mobile communication systems, non-orthogonal multiple access (NOMA) has recently been shown to be a promising candidate [5]-[9]. Exploiting different domains, e.g. power and/or code domains, rather than the traditional time and frequency domains, the NOMA technique allows several users to simultaneously utilize, the same frequency resources. An increased system spectral efficiency is therefore expected with the NOMA over the conventional orthogonal multiple access (OMA) [10]. Basically, the NOMA can be divided into three categories, including power-domain NOMA [11], code-domain NOMA [12], and hybrid NOMA [13]-[14]. Specifically, the power-domain NOMA (PD NOMA) is considered in this work for cooperative relaying to enhance the performance of the relay network in terms of outage probability, throughput and ergodic sum rate. In [15], the adaptation of the NOMA was shown to considerably outperform the conventional cooperative relaying techniques. In addition, the PD NOMA is considered in this paper due to the fact that it can eliminate the interference and serve multiple users simultaneously by applying superposition coding and successive interference cancellation (SIC). Moreover, in PD NOMA, the users are allocated different power levels to ensure the user fairness, i.e. the weak user is allocated more power than the strong user [16]-[17], which accordingly results in an enhanced quality of service for the SWIPT system.

In our previous work in [18], a simultaneous wireless information and power transfer (SWIPT) in a CRNOMA system was investigated. In [18], the power-splitting relaying (PSR) and time switching-based relaying (TSR) protocols are employed in the system. The work of [18] focused on the performance in terms of the outage probability, throughput and ergodic rate at low *SNR* region.

Dealing with energy issues in wireless networks, energy harvesting (EH) plays a critical role in different wireless network models because of the limited power supply and storage at transceivers, for instance in wireless sensor networks [19]-[22]. Several EH mechanisms were integrated into the devices to prolong the lifetime of energy-constrained wireless networks [23]-[25]. Such EH circuit integration enables the SWIPT to be applied in many areas such as healthcare, disaster, rescue, etc.

SWIPT can also be adapted in relay node based CRNOMA communications by employing either PSR or TSR protocol. In the PSR protocol, the received signal power at the relay node is divided into two parts by splitter. The one is for EH at the relay node and the other is for information processing (IP) to the destination node. In the TSR protocol, the RF received signal at the relay node is first sent to the EH receiver and then to the information receiver by switching. Therefore, a time block for EH and IP for the PSR protocol is normally divided into two time slots including the EH and data transmission during the first time slot and data forwarding in the remaining time slot. Otherwise, a time block for EH and IP for the TSR protocol is normally divided into three time slots including EH in the first time slot, data transmission from the source to the relay in the second time slot and data forwarding from the relay to the destination in the remaining time slot [26].

In [27], two PSR and TSR protocols for DF based relay networks were investigated. Specifically, both the PSR and TSR protocols were considered with and without the direct path. The outage probability expressions were presented. Also, the power splitting and time switching coefficients were optimized to maximize the transmission rate for the PSR and TSR protocols, respectively.

In [26], [28], SWIPT based relaying networks were presented. The expressions of the outage probability and ergodic capacity for amplify-and-forward (AF) and DF relaying protocols were derived. Moreover, these formulas provided practical insights into the impacts of several parameters on the SWIPT. These parameters include EH time, power splitting ratio, source to relay distance as well as EH efficiency. A radio-frequency EH scheme was also considered in [28] for cooperative relaying systems showing that the PSR obtains an enhanced throughput compared to the TSR at high *SNR*. In [29], a novel cooperative SWIPT NO-

MA protocol with PSR scheme was proposed. The data rate maximization of the user with poor channel conditions was investigated for multiple-input single-output cases. In [30], a SWIPT based DF relaying network was studied to derive approximate and exact closed-form expressions for outage probability. Furthermore, expressions for throughput in delay limited mode were given. In [31], a SWIPT-CRNOMA system was investigated. A novel PSR protocol for EH relay of this system was proposed and its impact on the outage probability of both users was considered. The outage probability and system throughput were derived for delay-sensitive transmission mode and their analytical expressions were also obtained. The application of SWIPT in CRNOMA was studied in [32] where novel analytical expressions of outage probability were derived both for the weak and strong users.

Taking into account signal processing at relay node, two transmission modes can be carried out, which include delay-limited transmission (DLT) and delay-tolerant transmission (DTT) modes [19]. In the DLT mode, the signal received at the destination node is decoded by block-wise signal decoding mechanism, while the received data blocks in the DTT mode can be stored in its buffer prior to data decoding.

In [33], a cooperative NOMA scheme with DLT and DTT modes employing DF relaying in full-duplex (FD) and HD modes was proposed. The new closed-form expressions for two types of exact and asymptotic outage probabilities as well as delay-limited throughput were derived. The FD CRNOMA obtained a higher EE than the HD CRNOMA in the DLT mode in the low *SNR* region. In contrast, the EE for HD CRNOMA was superior to that for FD CRNOMA in the DTT mode in the high *SNR* region.

DF is a protocol in which the received signal is decoded and forwarded to the desired destination, while AF is a protocol in which the received signal is first amplified and then forwarded to the destination. According to [34], the simultaneous transmissions from the source and active relay causes the inter-relay interference (IRI) to another receiving relay. In relay-assisted CNOMA network, AF relay protocol is normally employed in the models in which IRI condition is regardless [34]-[36]. It means that the AF relay protocol is usually utilized in multi-relay models or the information communication among relays. For DF relay protocol, it decodes the received data from the source by considering the IRI as noise component or decodes the IRI first by employing successive interference cancellation (SIC) [34]. This implies that the IRI has to be extremely weaker or stronger than the transmitted signal from the source.

In [37], the authors proposed two protocols, namely CNOMA-SWIPT-TS and

CNOMA-SWIPT-PS, based on TS and PS for system model with Nakagami-m fading channel. In the model, the source first sends transmitted signal to user UE1 and relay in phase one, then the relay forwards the signal to the user UE2 in phase two. The ergodic capacity and outage probability for the proposed protocols were evaluated and compared to that for OMA and the PS based protocol, namely EH and spectrum sharing protocol, in [38]. In particular, the sum ergodic capacity of CNOMA-SWIPT-PS was superior to OMA and the protocol in [38]. In [38], the authors proposed a new approach to solve the spectrum and power issues in wireless sensor network based on PSR protocol for Nakagami-m fading channel. This approach was the cooperation of spectrum sharing and RF EH. The outage probability was then evaluated for the primary and secondary systems. In [39], a hybrid SWIPT protocol combined PS and TS based architecture was investigated for CNOMA downlink transmission. The outage probability and channel capacity were derived and evaluated via simulation results. However, in general, energy efficiency issues and the impacts of the related parameters, e.g. the distance between the source and relay node and path loss factor, on the performance at high *SNR* region have not yet solved in these papers.

Inspired by the works in [19] and [33], in this paper, the employment of the PSR and TSR protocols for CRNOMA-based CRWPNs in both DLT and DTT modes is investigated. Additionally, it is motivated from our previous studies in [18], the energy efficiency of these two protocols and their impacts on the performance of the system model is continued investigating in this work. Furthermore, we investigate the system model with only one source (S), one relay (R) and one destination (D). Therefore, the DF relay protocol is exploited in this system model based on aforementioned analysis. The main contributions of the work can be summarised as follows:

- *PSR/TSR Protocols in DLT and DTT Modes*: PSR and TSR protocols are sequentially employed for SWIPT in a CRNOMA-based CRWPNs consisting of a source node and two destination nodes among which one plays the role as a relay node to assist the communication between the source and the far-end nodes. Additionally, DF is considered at the relay node over two transmission modes, i.e. DLT and DTT.

- *Performance Analyses*: Closed-form expressions of outage probability, throughput, ergodic rate and EE are derived for the PSR and TSR protocols with DLT and DTT modes in the CRNOMA-based CRWPNs. Next, the performance are analysed to realise the impacts of EH time, EH efficiency, power

splitting ratio, source data rate, and the distance between the nodes. Furthermore, the impacts of these parameters on the outage probability and ergodic rate of two users at high SNR region are also evaluated. The simulation results demonstrate that the performance for CRNOMA outperforms that for OMA. For performance comparison between two protocols, the TSR achieves higher throughtput, ergodic rate and EE than the PSR.

- For the first time, the investigation and evaluation of performance metric versus different distances between the source and relay node and comparison between direct and no-direct links with different path losses are performed.

- The PSR/TSR based system model in this work obtains a better outage probability than the work of [30].

The rest of the paper is structured as follows: Section II presents the entire system model of the proposed relay assisted cooperative NOMA and assumptions. Sections III, IV analyse the outage performance, throughput, ergodic rate and EE of the PSR and TSR protocols, respectively. Section V discusses the simulation results. Finally, Section VI concludes this paper and summarizes the key findings.

Notations: E[.] represents expectation operation. $f_X(Y)(.)$ and $F_X(Y)(.)$ represent the probability density function (PDF) and the cumulative distribution function (CDF) of a random variable X(Y), respectively. $|h_1|^2$ and $|h_2|^2$ denote channel gains. β, $0 < \beta < 1$, denotes the power splitting ratio.

2. SYSTEM MODEL

Figure 1 presents the system model under investigation. Here, a source node, S, wants to transfer the information to two users R and D. Assume that there is an obstacle between S and D as illustrated in Fig. 1, S sends two signals x_1, x_2 to R in phase 1, and R is exploited to help S to forward the decoded signal x_2 to D in phase 2. In this communication, R employs DF relaying protocol using the energy harvested from S. It is assumed that the links between nodes experience Rayleigh fading. d_1 and d_2 are the distances from S to R and from R to D, respectively. h_1 and h_2 are the complex channel coefficients of $S \to R$ and $R \to D$ links, respectively. These parameters have $|h_1|^2$ and $|h_2|^2$ which are assumed to be exponentially distributed with $E[|h_1|^2] = \Omega_1^{-1}$ and $E[|h_2|^2] = \Omega_2^{-1}$. In which, E[.] represents expectation operation. Without loss of generality, it is assumed that the fading gains in all related links are the Rayleigh distribution and their probability

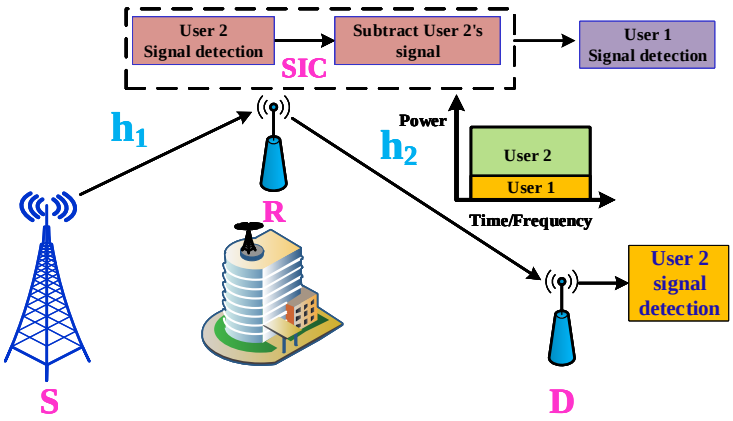

Figure 1: System Model.

density function (PDF) denotes by

$$f_{h_i}(x) = \frac{1}{\Omega_i}\exp(-\frac{x}{\Omega_i}),\ i \in \{1,2\}, \tag{1}$$

where, Ω_i represents the average power and the cumulative distribution function (CDF) is determined by:

$$F_{h_i}(x) = 1-\exp(-\frac{x}{\Omega_i}),\ i \in \{1,2\} \tag{2}$$

Moreover, the R and D are affected by Additive White Gassian Noise (AWGN) appearing at the RF-to-Baseband Conversion Unit (RFBCU) and the receiving antenna with the same variance N_0 [40].

2.1. Energy Harvesting and Information Processing at R

In this section, two protocols for EH at R, namely PSR-based R and TSR-based R, are sequentially considered. In addition, in the system model, [1]

2.1.1. Energy Harvesting at PSR-based R

The communication block diagram with the total block time T for EH and information processing (IP) in PSR protocol is plotted in Fig. 2. In this protocol,

[1] it is assumed that the energy consumption of data transmission which is generally much higher than that of data processing. Therefore, the amount of energy for data processing is implicitly negligible.

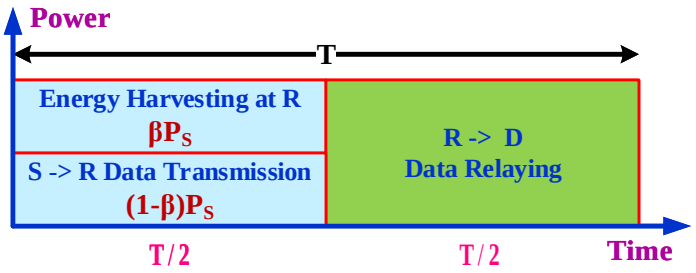

Figure 2: PSR Protocol of Energy harvesting system.

it is assumed that S transmits information to R during the first half of T, the remaining time of $T/2$ is utilized for transmitting the information from R to D. The transmitted signal at S is combined by two signals x_1 and x_2 employing superposition coding mechanism in NOMA [41].
The source S simultaneously transmits the superposed coding signal to R. The expectations of signals x_1 and x_2 are assumed that $E[x_1^2] = E[x_2^2] = 1$. Thus, the transmitted signal expression at S is given by

$$S(t) = \left(\sqrt{a_1 P_S} x_1(t) + \sqrt{a_2 P_S} x_2(t)\right) \tag{3}$$

where a_1 and a_2 denote the power allocation coefficients for data symbol x_1 and x_2, respectively. P_S represents the transmission power at S. The observed signal at R is given by

$$y_R(t) = h_1 S(t) + n_R(t) = h_1 \left(\sqrt{a_1 P_S} x_1(t) + \sqrt{a_2 P_S} x_2(t)\right) + n_R(t), \tag{4}$$

where $n_R(t)$ AWGN at R with zero mean and variance N_0. Since R is nearer to S than D, the power is allocated for R less than that for D to ensure the user fairness. Thus, $a_2 > a_1 > 0$ satisfies $a_1 + a_2 = 1$. Following the power splitting architecture at R [26, Fig.(3b)], the received power at R is splitted into two parts as follows: i) $\sqrt{\beta} y_R$ is exploited to harvest the energy and ii) $\sqrt{1-\beta} y_R$ is used to process information. Let β, $0 < \beta < 1$, denote the power splitting ratio. The received power at R to harvest the energy is given as

$$y_{H,R}(t) = \sqrt{\beta} y_R(t) = \sqrt{\beta} h_1 \left(\sqrt{a_1 P_S} x_1(t) + \sqrt{a_2 P_S} x_2(t)\right) + \sqrt{\beta} n_R(t) \tag{5}$$

The harvested energy at R can be determined by

$$E_H^{PSR} = \beta \eta |h_1|^2 P_S (T/2), \tag{6}$$

where $0<\eta<1$ denotes the EH efficiency at the energy receiver and depends on the rectifier and EH circuitry deployed at R. For harvested energy at R, a part is used consuming at R while the remaining part is used for DF the received signal to D. The transmission power at R depends on E_H^{PSR} and is determined by

$$P_r^{PSR} = \frac{E_H^{PSR}}{(T/2)} = \frac{\beta\eta|h_1|^2 P_S (T/2)}{(T/2)} = \beta\eta|h_1|^2 P_S. \tag{7}$$

.

2.1.2. Information Processing at PSR-based R

The received signal at R to process information is given as

$$\begin{aligned} y_{IPPSR,R}(t) &= \sqrt{1-\beta}\, y_R(t) \\ &= \sqrt{1-\beta}\, h_1 \left(\sqrt{a_1 P_S}\, x_1(t) + \sqrt{a_2 P_S}\, x_2(t)\right) + \sqrt{1-\beta}\, n_R(t). \end{aligned} \tag{8}$$

The data $y_{IPPSR,R}(t)$ is converted to a sampled baseband data $y_{IPPSR,R}(k)$ by the RFBCU at R. Similar to [26, Eq.(20)], $y_{IPPSR,R}(k)$ can be expressed as

$$\begin{aligned} y_{IPPSR,R}(k) &= \sqrt{1-\beta}\, y_R(k) \\ &= \sqrt{1-\beta}\, h_1 \left(\sqrt{a_1 P_S}\, x_1(k) + \sqrt{a_2 P_S}\, x_2(k)\right) + \sqrt{1-\beta}\, n_R(k) + n_R^c(k), \end{aligned} \tag{9}$$

where $n_R^c(k)$ is AWGN at the RFBCU of R.

2.1.3. Energy Harvesting at TSR-based R

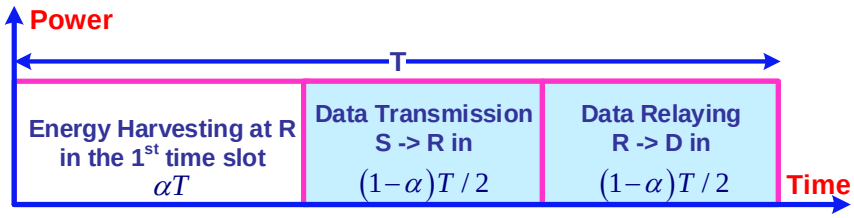

Figure 3: TSR Protocol of Energy harvesting system.

Similar to PSR protocol, the communication block diagram with the total block time T for EH and IP in TSR protocol is plotted in Fig. 3. The first sub-block of time, i.e. αT, is for EH, the first half of the remaining block,

i.e. $(1-\alpha)T/2$, is for the data transmission from S to R and then the remaining $(1-\alpha)T/2$ is for the data transmission from R to D. Let α, $0<\alpha<1$, denote the time allocation ratio.

Based on the time switching architecture for EH and IP at relay [26, Fig.(2b)], R harvests the energy from the received RF signal during the first sub-block of time αT as in (1), i.e.

$$E_H^{TSR} = \alpha\eta|h_1|^2 P_S T. \tag{10}$$

Then, the normalized transmission power at R can be obtained from the harvested energy E_H^{TSR} over the time $(1-\alpha)T/2$ for forwarding the decoded signal to D as

$$P_r^{TSR} = \frac{E_H^{TSR}}{(1-\alpha)T/2} = \frac{\alpha\eta|h_1|^2 P_S T}{(1-\alpha)T/2} = \frac{2\alpha\eta|h_1|^2 P_S}{(1-\alpha)}. \tag{11}$$

According to the NOMA principle, R is allocated less power than D. After receiving the combined signal from S, R decodes the signal x_2 and decodes its own signal x_1 by applying SIC [42].

2.1.4. Information Processing at TSR-based R

To decode the data of the source S, the RFBCU at R converts the received RF data $y_R(t)$ in Eq. (1) into a sampled baseband data $y_{IPTSR,R}(k)$ in the first interval time $(1-\alpha)T/2$. The sampled signal $y_{IPTSR,R}(k)$ is explicitly expressed as follows [26, Eq. (3)].

$$y_{IPTSR,R}(k) = h_1\left(\sqrt{a_1 P_S}x_1(k) + \sqrt{a_2 P_S}x_2(k)\right) + n_R(k) + n_R^c(k). \tag{12}$$

Considering both PSR and TSR protocols, from (9) and (12), the received signal to interference plus noise ratio ($SINR$) at R for detecting x_2 of D can be expressed by

$$\gamma_{2,R} = \frac{\psi_I|h_1|^2 a_2\rho}{\psi_I|h_1|^2 a_1\rho + 1}, \tag{13}$$

where $\rho \triangleq \frac{P_S}{N_0}$ is the transmitting SNR, ψ_I represents the IP coefficient in the PSR and TSR protocols which is given by

$$\psi_I = \begin{cases} \frac{(1-\beta)}{(2-\beta)}, & for\ PSR. \\ \\ \frac{1}{2}, & for\ TSR. \end{cases} \tag{14}$$

The received *SNR* at R for detecting its own message x_1 after SIC is expressed by

$$\gamma_{1,R} = \psi_I |h_1|^2 a_1 \rho. \tag{15}$$

After decoded at R, the signal x_2 is forwarded to D. The received signal at D can be given by

$$y_D(t) = \sqrt{P_r^X} x_2(t) h_2 + n_D(t), \tag{16}$$

where X is either PSR or TSR, $n_D(t)$ denotes AWGN at D with zero mean and variance N_0. The signal $y_D(t)$ is converted to a sampled baseband data $y_D(k)$ by the RFBCU at D.

$$y_D(k) = \sqrt{P_r^X} x_2(k) h_2 + n_D(k) + n_D^c(k), \tag{17}$$

where $n_D^c(k)$ is AWGN at the RFBCU of D.
By substituting (7) and (9) into (17), the expression becomes

$$y_D(k) = \left(\sqrt{\psi_E P_S}\right) |h_1| h_2 x_2(k) + n_D(k) + n_D^c(k), \tag{18}$$

where ψ_E denotes the EH coefficient in the PSR and TSR protocols and is given by

$$\psi_E = \begin{cases} \beta\eta, & for\ \ PSR. \\ \\ \frac{2\alpha\eta}{(1-\alpha)}, & for\ \ TSR. \end{cases} \tag{19}$$

The received *SNR* at D is thus given by

$$\gamma_{2,D} = \frac{|h_1|^2 |h_2|^2 \psi_E P_S}{2N_0} = \frac{1}{2} |h_1|^2 |h_2|^2 \psi_E \rho. \tag{20}$$

3. PERFORMANCE ANALYSIS OF PSR PROTOCOL

3.1. Outage Performance

3.1.1. Outage Probability at R

In the CRNOMA scheme, R is not in outage when it can decode both x_1 and x_2. Thus, the outage probability at R can be given by

$$P_{R,PSR} = 1 - \Pr\left(\gamma_{2,R} > \gamma_{th_2}, \gamma_{1,R} > \gamma_{th_1}\right), \tag{21}$$

where $\gamma_{th_1} = 2^{2R_1} - 1$ and $\gamma_{th_2} = 2^{2R_2} - 1$. Here, R_1 and R_2 denote the target rates for detecting x_1 and x_2, respectively. The following finding of the outage probability at R is given by Theorem 1.

Theorem 1. *The outage probability at R of PSR protocol is given by*

$$P_{R,PSR} = 1 - e^{-\frac{\theta_{1,PSR}}{\Omega_1}}, \tag{22}$$

where $\theta_{1,PSR} = \max(\tau_{1,PSR}, \nu_{1,PSR})$, $\tau_{1,PSR} = \frac{\gamma_{th2}}{\rho \psi_I^{PSR}(a_2 - a_1\gamma_{th2})}$ *and* $\nu_{1,PSR} = \frac{\gamma_{th1}}{a_1 \psi_I^{PSR} \rho}$ *with* $a_2 > a_1\gamma_{th2}$.
Proof:
See Appendix A.

3.1.2. Outage Probability at D

Similarly, the outage probability at D occurs when R cannot detect x_2 to forward to D or R can detect x_2 but D cannot recover x_2 and is thus given by

$$P_{D,PSR} = \Pr(\gamma_{2,R} < \gamma_{th_2}) + \Pr(\gamma_{2,D} < \gamma_{th_2}, \gamma_{2,R} > \gamma_{th_2}) \tag{23}$$

Theorem 2. *The outage probability at D of PSR protocol can be computed by*

$$P_{D,PSR} = 1 - e^{-\frac{\tau_{1,PSR}}{\Omega_1}} + \int_{\tau_{1,PSR}}^{\infty} \left(1 - \mathrm{e}^{\frac{-2\gamma_{th_2}}{x\psi_E^{PSR}\rho\Omega_2}}\right) \frac{1}{\Omega_1} \exp\left(\frac{-x}{\Omega_1}\right) dx \tag{24}$$

Proof:
See Appendix B.

Corollary 1. *The outage probability at D at high SNR is determined as follows*

$$\begin{aligned} P_{D,PSR}^{\infty} &= \Pr\left(\frac{a_2}{a_1} < \gamma_{th_2}\right) + \Pr\left(|h_2|^2 < \frac{2\gamma_{th_2}}{\psi_E^{PSR}\rho|h_1|^2}, \frac{a_2}{a_1} > \gamma_{th_2}\right) \\ &= \Pr\left(|h_2|^2 < \frac{2\gamma_{th_2}}{\psi_E^{PSR}\rho|h_1|^2}, \frac{a_2}{a_1} > \gamma_{th_2}\right) \\ &= \int_0^{\infty} \left[1 - \exp\left(\frac{-2\gamma_{th_2}}{\psi_E^{PSR}\rho\Omega_2 x}\right)\right] \frac{1}{\Omega_1} \exp\left(\frac{-x}{\Omega_1}\right) dx \\ &= 1 - 2\sqrt{\frac{2\gamma_{th_2}}{\psi_E^{PSR}\rho\Omega_1\Omega_2}} K_1\left(2\sqrt{\frac{2\gamma_{th_2}}{\psi_E^{PSR}\rho\Omega_1\Omega_2}}\right), \end{aligned} \tag{25}$$

where $K_1(.)$ *is the first order modified Bessel function of the second kind* [43, $Eq.(3.324.1)$].

3.2. Throughput for Delay-limited Transmission Mode

In DLT mode, S transmits x_1 and x_2 with constant rates of R_1 and R_2, respectively. The throughput therefore depends only on the outage probability caused by wireless fading channels, which is computed by

$$\tau_{t,PSR} = \left(1 - P_{R,PSR}\right) R_1 + \left(1 - P_{D,PSR}\right) R_2, \tag{26}$$

where $P_{R,PSR}$ and $P_{D,PSR}$ can be obtained from (22) and (26), respectively.

3.3. Ergodic Rate for Delay-tolerant Transmission Mode

In DTT mode, ergodic rate is analysed instead of throughput since the throughput depends on the ergodic capacity, which in turn depends on power splitting factor for the PSR protocol and EH time for the TSR protocol [26]. In the following, the ergodic rates at R and D are sequentially evaluated.

3.3.1. Ergodic Rate at R

The achievable rate at R when R can detect x_2 is given by [33]

$$\begin{aligned} R_{R,PSR} &= E\left[\tfrac{1}{2}\log_2\left(1+\gamma_{1,R}\right)\right] \\ &= \tfrac{1}{2}\int_0^{\infty} \log_2\left(1+\gamma_{1,R}\right) f\left(\gamma_{1,R}\right) d\gamma_{1,R} \end{aligned} \tag{27}$$

Theorem 3. *The ergodic rate at PSR-based R in DTT mode is determined by*

$$R_{R,PSR} = \frac{-\exp\left(\frac{1}{\psi_I^{PSR} a_1 \rho \Omega_1}\right)}{2\ln 2} Ei\left(\frac{-1}{\psi_I^{PSR} a_1 \rho \Omega_1}\right), \tag{28}$$

where $Ei(.)$ denotes the exponential integral function [43, $Eq.(3.354.4)$].
Proof:
See Appendix C.

3.3.2. Ergodic Rate at D

The achievable rate at D for PSR with DTT mode is given by

$$R_{D,PSR} = \frac{1}{2}\log_2\left(1+\min\left(\gamma_{2,R}, \gamma_{2,D}\right)\right). \tag{29}$$

Theorem 4. *The ergodic rate at D for PSR protocol with DTT mode is given by*

$$R_{D,PSR} = \frac{1}{2\ln 2}\int_0^{\frac{a_2}{a_1}} \left[\frac{e^{-\frac{x}{\psi_I^{PSR}\rho(a_2-a_1x)\Omega_1}}}{1+x} + \frac{\int_{\frac{x}{\psi_I^{PSR}\rho(a_2-a_1x)}}^{\infty} \frac{1}{\Omega_1}\left(1-e^{-\frac{2x}{y\rho\psi_E^{PSR}\Omega_2}}\right)e^{-\frac{y}{\Omega_1}}dy}{1+x} \right] dx. \tag{30}$$

Proof:
See Appendix D.

Remark 1. *The ergodic rate at high SNR is given by*

$$R_{D,PSR}^{\infty} = \frac{1}{2\ln 2}\int_0^{\infty} \frac{1-F_X(x)}{1+x}dx. \tag{31}$$

From the analytical result in (27)*, the asymptotic expression of the ergodic rate at D in case of the high SNR region* $\rho \to \infty$ *is expressed by*

$$R_{D,PSR}^{\infty} = \frac{1}{2\ln 2}\int_0^{\frac{a_2}{a_1}} \frac{2\sqrt{\frac{2x}{\psi_E^{PSR}\rho\,\Omega_1\Omega_2}}K_1\left(2\sqrt{\frac{2x}{\psi_E^{PSR}\rho\,\Omega_1\Omega_2}}\right)}{1+x}dx. \tag{32}$$

Proof:
See Appendix E.

3.3.3. Ergodic rate of the system

In summary, the ergodic rate for PSR in DTT mode is expressed by

$$\tau_{r,PSR} = R_{R,PSR} + R_{D,PSR}, \tag{33}$$

where $R_{R,PSR}$ and $R_{D,PSR}$ can be obtained from (33) and (35), respectively.

3.4. *Energy efficiency*

The EE is defined as the ratio of the total achievable data rate and the total power consumption in the entire network, which is given by EE $\stackrel{\Delta}{=} \frac{\Re}{P_S+P_r}$, where $\Re$, denotes the total throughput from S to R and from R to D and (P_S+Pr) denotes the total power consumption including the transmitted power P_S at S and the transmitted power P_r at R. Following [33, Eqs. (52) and (54)], the EE can be derived. Hence, the EE of user cooperative relaying for NOMA systems can be given by

$$EE_{\phi,PSR} = \frac{2\tau_{\phi,PSR}}{TP_S+TP_r} = \frac{2\tau_{\phi,PSR}}{\rho(1+\psi_E\,\Omega_1)}, \tag{34}$$

where $T=1, \sigma^2=1, \rho \stackrel{\Delta}{=} \frac{P_S}{\sigma^2}, P_r = \beta\eta|h_1|^2 P_S = \psi_E \Omega_1 P_S$ and $\phi \in (t,r)$ denotes the system energy efficiency in DLT mode and DTT mode, respectively.

4. PERFORMANCE ANALYSIS OF TSR PROTOCOL

4.1. *Outage performance*

The outage probabilities at R and D are derived as in the following two theorems.

Theorem 5. *The outage probability at R of TSR protocol is given by*

$$P_{R,TSR} = 1 - e^{-\frac{\theta_{1,TSR}}{\Omega_1}}, \tag{35}$$

where $\theta_{1,TSR} = \max(\tau_{1,TSR}, \nu_{1,TSR})$, $\tau_{1,TSR} = \frac{\gamma_{th2}}{\rho\psi_I^{TSR}(a_2-a_1\gamma_{th2})}$ *and* $\nu_{1,TSR} = \frac{\gamma_{th1}}{a_1\psi_I^{TSR}\rho}$ *with* $a_2 > a_1\gamma_{th2}$.
Proof:
See Appendix A.

Theorem 6. *The outage probability at D can be given by*

$$P_{D,TSR} = 1 - e^{-\frac{\tau_{1,TSR}}{\Omega_1}} + \int_{\tau_{1,TSR}}^{\infty} \left(1 - \mathrm{e}^{\frac{-2\gamma_{th_2}}{x\psi_E^{TSR}\rho\Omega_2}}\right) \frac{1}{\Omega_1} \exp\left(\frac{-x}{\Omega_1}\right) dx. \tag{36}$$

Proof:
See Appendix B.

Corollary 2. *The outage probability at D at high SNR can be determined by*

$$\begin{aligned} P_{D,TSR}^{\infty} &= \Pr\left(\tfrac{a_2}{a_1} < \gamma_{th_2}\right) + \Pr\left(|h_2|^2 < \tfrac{2\gamma_{th_2}}{\psi_E^{TSR}\rho|h_1|^2}, \tfrac{a_2}{a_1} > \gamma_{th_2}\right) \\ &= \Pr\left(|h_2|^2 < \tfrac{2\gamma_{th_2}}{\psi_E^{TSR}\rho|h_1|^2}, \tfrac{a_2}{a_1} > \gamma_{th_2}\right) \\ &= \int_0^{\infty} \left[1 - \exp\left(\tfrac{-2\gamma_{th_2}}{\psi_E^{TSR}\rho\Omega_2 x}\right)\right] \tfrac{1}{\Omega_1} \exp\left(\tfrac{-x}{\Omega_1}\right) dx \\ &= 1 - 2\sqrt{\tfrac{2\gamma_{th_2}}{\psi_E^{TSR}\rho\Omega_1\Omega_2}} K_1\left(2\sqrt{\tfrac{2\gamma_{th_2}}{\psi_E^{TSR}\rho\Omega_1\Omega_2}}\right), \end{aligned} \tag{37}$$

where $K_1(.)$ denotes the first order modified Bessel function of the second kind [43, $Eq.(3.324.1)$].

4.2. Throughput for Delay-limited Transmission Mode

The total system throughput for TSR in DLT mode can be similarly derived as

$$\tau_{t,TSR} = \left(1 - P_{R,TSR}\right) R_1 + \left(1 - P_{D,TSR}\right) R_2, \tag{38}$$

where $P_{R,TSR}$ and $P_{D,TSR}$ can be obtained from (40) and (41), respectively.

4.3. Ergodic Rate for Delay-tolerant Transmission Mode

4.3.1. Ergodic Rate at R

When R can detect signal x_2, the achievable rate at R can be obtained by [33]

$$R_{R,TSR} = \frac{1}{2}\log_2\left(1 + \gamma_{1,R}\right). \tag{39}$$

Theorem 7. *The ergodic rate at R for CRNOMA is given by*

$$R_{R,TSR} = \frac{-\exp\left(\frac{1}{\psi_I^{TSR} a_1 \rho \Omega_1}\right)}{2\ln 2} Ei\left(\frac{-1}{\psi_I^{TSR} a_1 \rho \Omega_1}\right), \tag{40}$$

where $Ei(.)$ is the exponential integral function [43, $Eq.(3.354.4)$].
Proof:
See Appendix C.

4.3.2. Ergodic Rate at D

The achievable rate at D is given by

$$R_{D,TSR} = \frac{1}{2}\log_2\left(1+\min\left(\gamma_{2,R},\gamma_{2,D}\right)\right). \tag{41}$$

Theorem 8. *The ergodic rate at D is given by*

$$R_{D,TSR} = \frac{1}{2\ln 2}\int_0^{\frac{a_2}{a_1}}\left[\frac{e^{-\frac{x}{\psi_I^{TSR}\rho(a_2-a_1x)\Omega_1}}}{1+x} + \frac{\int_{\frac{x}{\psi_I^{TSR}\rho(a_2-a_1x)}}^{\infty}\frac{1}{\Omega_1}\left(1-e^{-\frac{2x}{y\rho\psi_E^{TSR}\Omega_2}}\right)e^{-\frac{y}{\Omega_1}}dy}{1+x}\right]dx \tag{42}$$

Proof:
See Appendix D.

Remark 2. *The ergodic rate at high SNR is given by*

$$R_{D,TSR}^{\infty} = \frac{1}{2\ln 2}\int_0^{\infty}\frac{1-F_X(x)}{1+x}dx. \tag{43}$$

From (48), the asymptoic expression of ergodic rate at D for high SNR region $\rho\to\infty$ is given by

$$R_{D,TSR}^{\infty} = \frac{1}{2\ln 2}\int_0^{\frac{a_2}{a_1}}\frac{2\sqrt{\frac{2x}{\psi_E^{TSR}\rho\,\Omega_1\Omega_2}}K_1\left(2\sqrt{\frac{2x}{\psi_E^{TSR}\rho\,\Omega_1\Omega_2}}\right)}{1+x}dx. \tag{44}$$

Proof:
See Appendix E.

4.3.3. Ergodic rate of the system

In summary, the ergodic rate for TSR in DTT mode is given by

$$\tau_{r,TSR} = R_{R,TSR} + R_{D,TSR} \tag{45}$$

where $R_{R,TSR}$ and $R_{D,TSR}$ can be obtained from (45) and (47), respectively.

*4.4. **Energy efficiency***

Similar to the derivation of the EE for the PSR protocol in CRNOMA system (see Section 3), the EE of the TSR protocol can be determined by

$$EE_{\phi,TSR} = \frac{2\tau_{\phi,TSR}}{\rho\left(1+\psi_E\Omega_1\right)}, \tag{46}$$

where $\phi \in (t,r)$, denotes the system energy efficiency in DLT mode and DTT mode, respectively.

5. SIMULATION RESULTS

In this section, the Matlab software is utilized to simulate the system model scenarios for verifying provided results and confirming our analytical expressions contained in the preceding sections. Without loss of generality, in our model, the simulation parameters are assumed and chosen as follows: the distance between S and D is normalized to unity, i.e. $\Omega_{SD} = 1, \Omega_{SR} = d^{-m}$ and $\Omega_{RD} = (1-d)^{-m}$, where d is the normalized distance between the S and R, with $d = 0.3$ and m is pathloss exponent, with $m = 2$. The power allocation coefficients of CRNOMA are set $a_1 = 0.2$ and $a_2 = 0.8$ for R and D, respectively. The target rates of R_1 and R_2 are 3 and 0.5 bps/Hz, respectively.

In the simulation, the performance of the traditional OMA is used as a counterpart for comparison. Specifically, in the OMA scheme, during the first time slot of the time block, S sends the information x_1 to user relay R and then (i.e. the second time slot) sends x_2 to R. Finally, during the third time slot of the time block, R decodes and forwards the information x_2 to D. In addition, [30] is utilized as a benchmark for the comparison of the outage probability. In [30], the source transmits a signal x_1 to relay and destination nodes in the first time slot. At the same time, the relay also performs energy harvesting from the received signal. Then, the source transmits another signal x_2 to the destination node and R also forward the signal x_1 to this destination node in the second time slot.

The outage performance and ergodic rate of both protocols are first analysed to realize the impacts of energy harvesting time, energy harvesting efficiency, power splitting ratio, source data rate, and the distance between the source and relay nodes.

Specifically, Figs 4(a)-(c) and 5(a)-(c) illustrate the outage probability of two users for the PSR and TSR protocols versus SNR, β and α, respectively. It can be observed that User 2 achieves a lower outage probability than that of User 1 in the

CRNOMA scheme as well as in the OMA scheme. Also, the outage probability of two users in the CRNOMA scheme is shown to be lower than those in the OMA scheme.

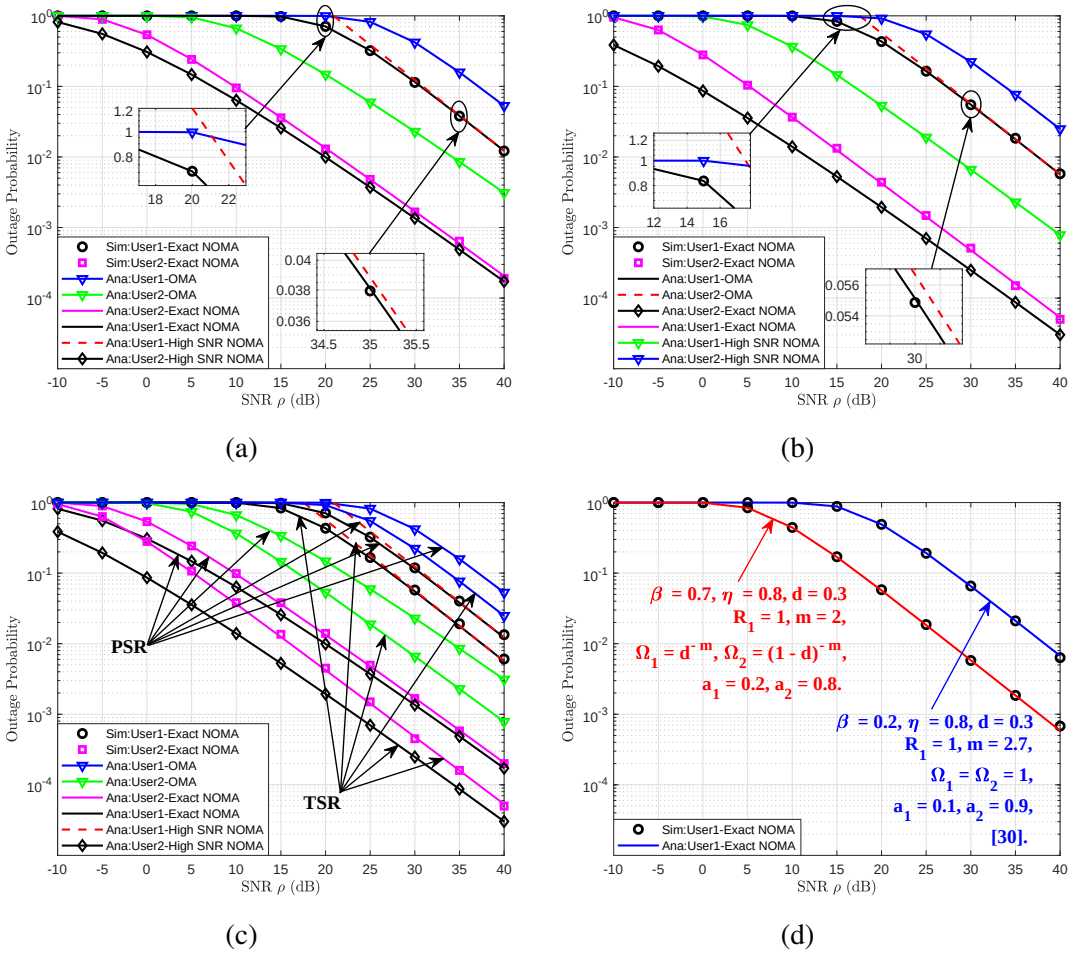

Figure 4: Outage probability versus transmitting *SNR* for (a) PSR protocol, (b) T-SR protocol, (c) PSR and TSR protocols and d) Comparison of outage probability between this work and [30].

More specifically, in Figs 4(a)-(c) with $\beta = 0.7$, $\alpha = 0.7$, $\eta = 0.8$, $d = 0.3$, $m = 2$, $a_1 = 0.2$, $a_2 = 0.8$, $a_{1\_OMA} = 0.5$ and $a_{2\_OMA} = 0.5$, the outage probabilities of the PSR and TSR protocols are as a function of SNR (dB). From the figures, the probabilities of User1-exact and User1-High of PSR protocol are significantly

higher than that of the TSR protocol. When SNR increases, the probability of PSR and TSR protocols tends to decrease linearly. It means that as the signal is stronger than noise, the successfully sent data will be higher. Furthermore, figure 4(d) describes the comparison in terms of outage probability for User1-exact of CRNOMA scheme between our work and the work of [30]. The figure shows that the protocols for our work obtain a lower outage probability than that for the work of [30]. It can be concluded that the higher the target rate, the higher the dropped data. In general, the protocols in our work are better than that in the work of [30].

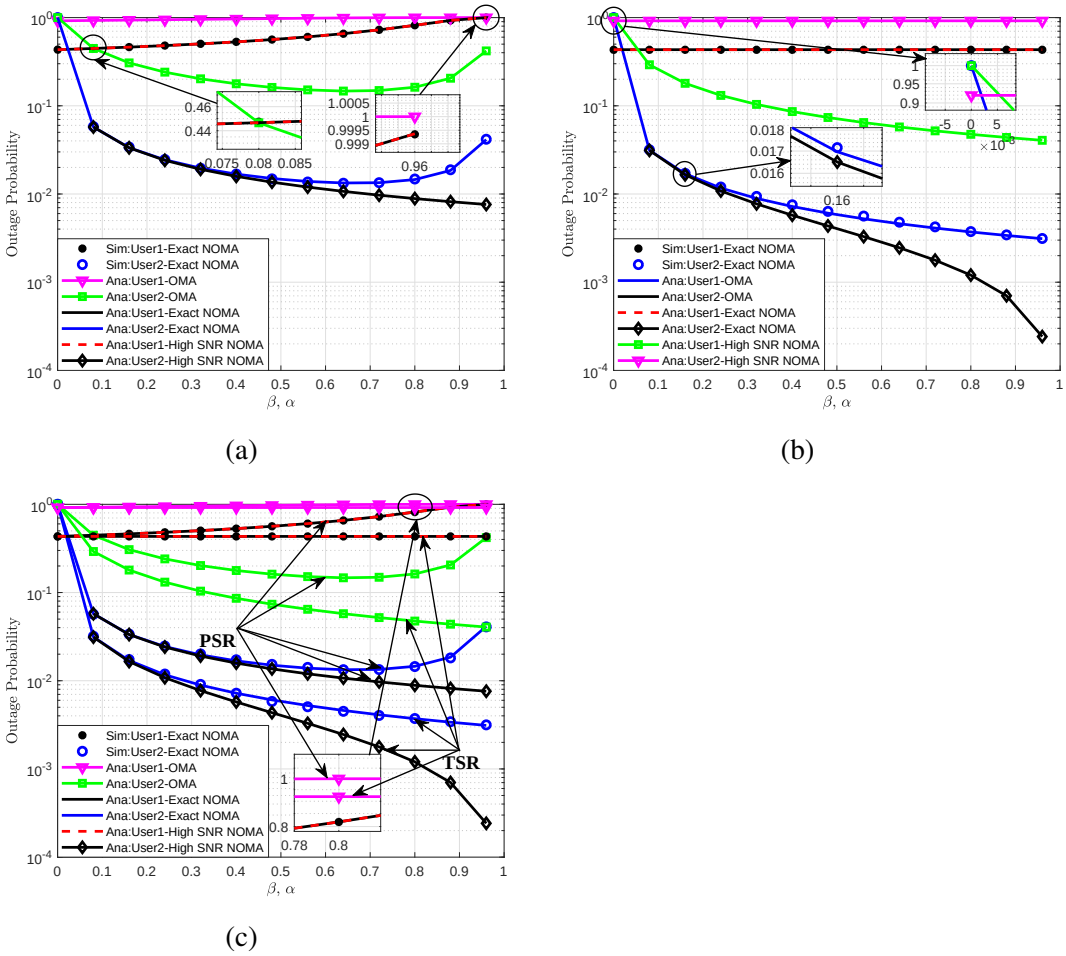

Figure 5: Outage probability versus the transmitting energy harvesting coefficients for (a) PSR protocol, (b) TSR protocol and (c) PSR and TSR protocols.

Figure 5 plots the outage probability of two users for the PSR and TSR protocols versus α and β. The α and β values vary from of 0 to 1. As shown in the figure, the outage probability of User 2 is lower than that of User 1 for the both PSR and TSR protocols. Also, the outage probability of both users for TSR protocol is lower than the one for PSR protocol. In α range of from 0 to 0.3, the outage probability of User 2 for both CRNOMA and OMA decreases strongly but the one of User 1 increases insignificantly. Similarly, in α range of from 0.3 to around 0.7, the outage probability of User 2 decreases gradually while the one of User 1 increases linearly. However, in remaining α range, the outage probability of User 2 for PSR based CRNOMA and OMA schemes tends to increase while the one for TSR based CRNOMA and OMA schemes still decreases gradually. These can be explained based on (22), (26), (40) and (41). In general, one can see clearly that the outage probability of the system can obtain well as α and β values are in range of from 0.3 to 0.7.

Figures 6(a)-(c) and 7(a)-(c) describe the throughput and ergodic rate of two users for the PSR and TSR protocols as a function of the β (β=α), where β on the x-axis is set from 0.001 to 1 with 0.08 step. Specifically, it can be seen in Figs 6(a)-(c) that the throughput of User 1 is much higher than that of User 2 in the CRNOMA scheme. This is due to the fact that R receives both x_1 and x_2 signals while D receives only x_2 in the DLT mode. One can observe from the figure that throughput of User 1 for TSR is almost constant while that for PSR decreases significantly when β increases. This demonstrates that the throughput of User 2 for PSR depends on β but that for TSR is not effected by β. It can be explained based on (14). The graphs also show that the TSR protocol achieves a better throughput as compared to the PSR protocol. Moreover, the throughput for the CRNOMA is also better than that of the OMA. The exact theoretical curves of the throughput of two users for the CRNOMA are plotted according to (31), (43), respectively.

Similarly, Figs 7(a)-(c) show that the ergodic rate at User 1 is higher than that at User 2 in the CRNOMA scheme. The ergodic rate at User 1 is the highest in the CRNOMA scheme, while the one at User 2 is the lowest in the OMA scheme. This means that the ergodic rate at R used to detect x_1 and x_2 in Eqs. (32), (33), (44), (45) is higher than the minimum value of at R used to detect x_2 and at D used to detect x_2 in Eqs. (34), (35), (46), (47), respectively. Compared between TSR and PSR protocols, the ergodic rate of both users for TSR is superior to that for TSR. Similar to the throughput, the ergodic rate for TSR is almost constant while that for PSR varies with β. The exact theoretical curves of the ergodic rate of two users for the CRNOMA are described according to equations (32)-(35) and

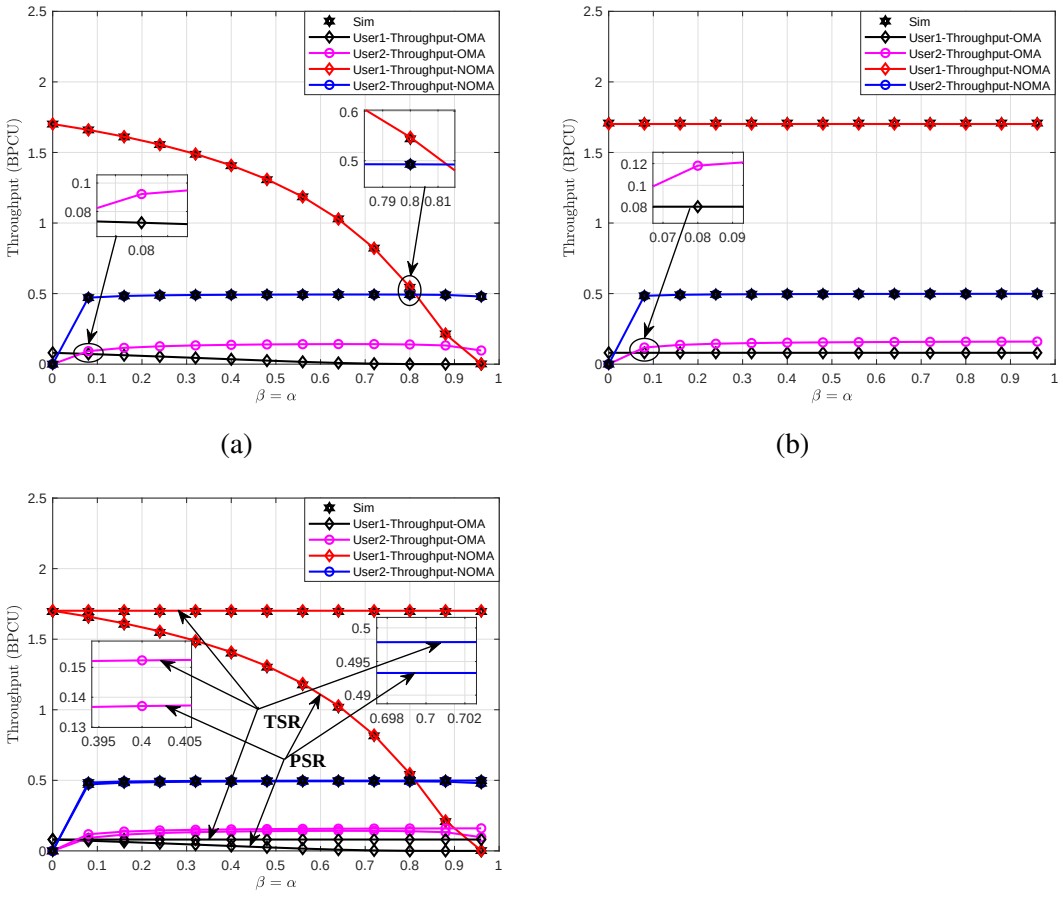

Figure 6: The throughput of two users versus $\beta = \alpha$ for (a) PSR protocol, (b) TSR protocol and (c) PSR and TSR protocols.

(44)-(47), respectively.

Figures 8(a)-(c) plots the energy efficiency of two users for the PSR and TSR protocols as a function of SNR (dB). It can be seen that the EE performance for the DLT mode is lower than that for the DTT mode. Thus, the NOMA outperforms the EE performance as compared to the conventional OMA in low SNR region ($< 10(dB)$). The reason is that the CRNOMA can achieve a larger throughput and ergodic rate than that of the OMA. The exact theoretical curves of the ergodic rate of two users for the CRNOMA are plotted according to (39) and (51). One

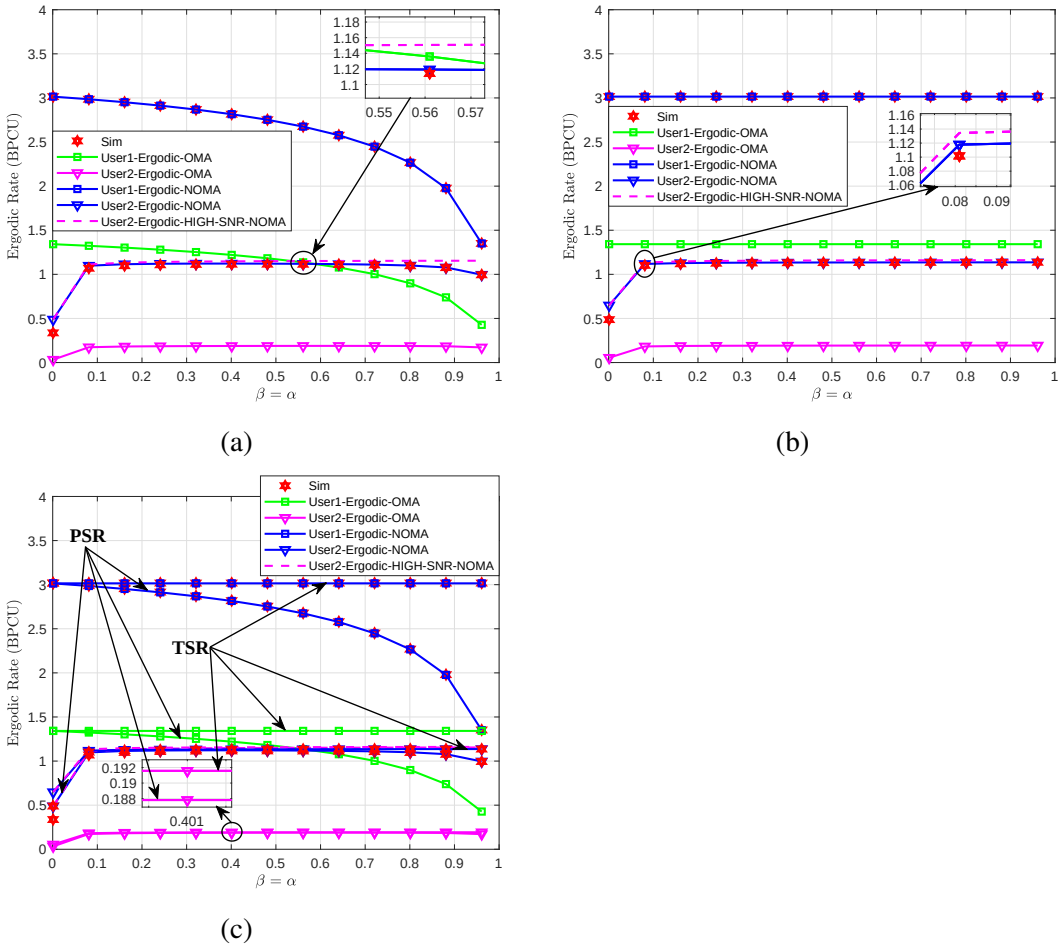

Figure 7: The ergodic rate of two users versus $\beta = \alpha$ for (a) PSR protocol, (b) TSR protocol and (c) PSR and TSR protocols.

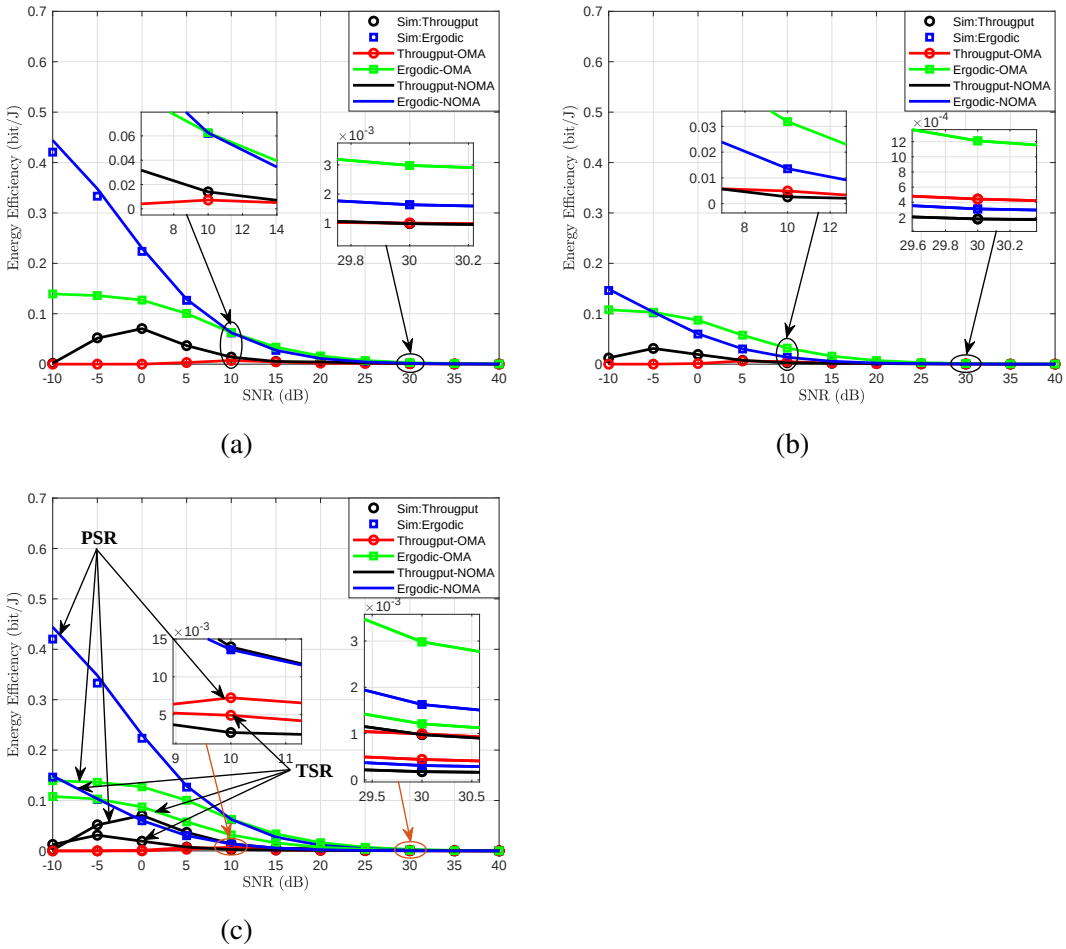

Figure 8: Energy efficiency of two users for (a) PSR protocol, (b) TSR protocol and (c) PSR and TSR protocols.

can observe that there is the occurrence of some inflection points in the figure. It can be explained that when the value of SNR is in lower range, the EE decreases rapidly. Again, the graph of EE varies towards gradually decreasing as SNR values are towards increasing according to (39) and (51). Thus, the existence of the inflection points in the figure is obvious. Moreover, from the figures 8(a)-(c) as well as in (39) and (51), they are shown that the EE versus throughput for DLT mode changes quickly and depends on (1/exp) term in (31) and (43) with $a_1 = 0.2$, $a_2 = 0.8$. The EE of the OMA system varies according to function F (1/exp)) with

$a_{1\_OMA} = 0.5$ and $a_{2\_OMA} = 0.5$. For explanation about the relationship between the EE and ergodic rate of the system, based on (38) and (43), it is noted that the EE of CRNOMA system decreases more and more according to 1/(2ln2) term in (38) and (43) while the EE of OMA system varies slowly according to function F (1/(3ln2)). As a result, some intersection and inflection points exist among the curves in the figures. Additionally, compared to the TSR, the PSR protocol obtains a higher EE.

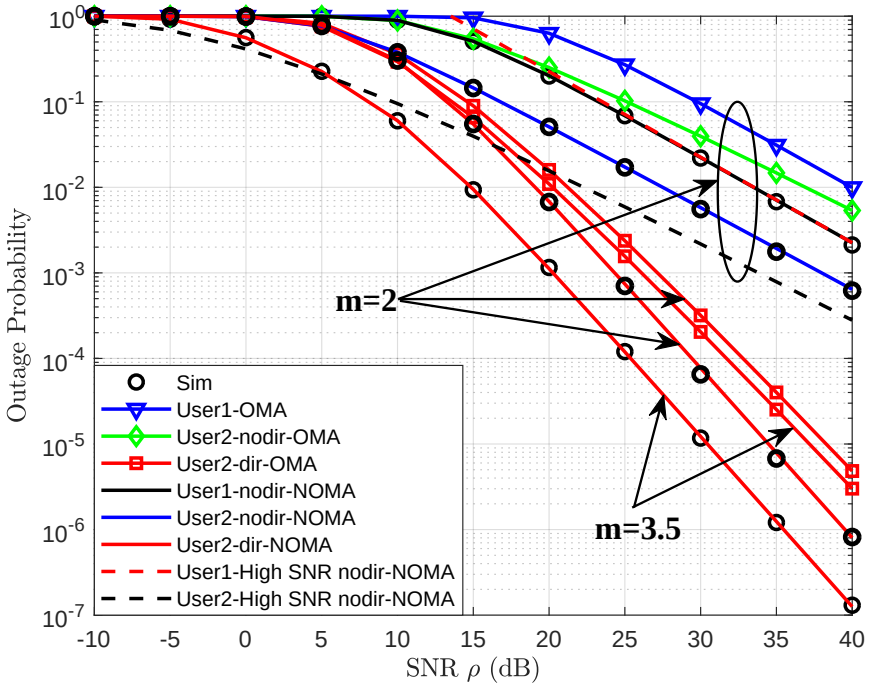

Figure 9: The outage probability versus *SNR* and different values of m.

Figure 9 plots the outage probability transmitting *SNR* according to different values of path loss factor m, i.e. $m = 2$ and $m = 3.5$, in cases of relay and direct links, respectively. One see from figure that the outage probability of User 2 in case of direct link for NOMA is lowest among these curves for both OMA and NOMA as well as direct link and relay link. The outage probability in case of relay communications with no direct link is higher than that of the case with direct link for both NOMA and OMA.

It can be observed from the Fig. 10 that the larger the distance d, the higher the outage probability of two users with NOMA. This implies that the quality of propagation path of the system is weak more and more. The reason is that the path

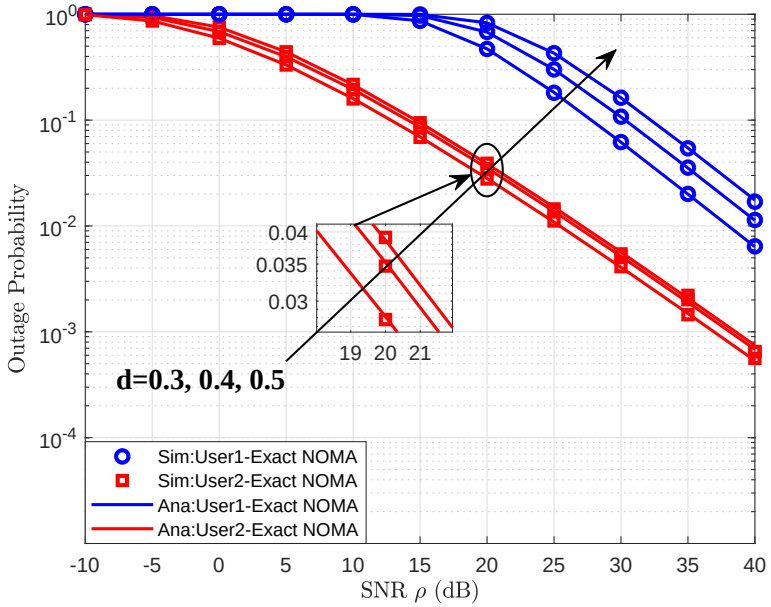

Figure 10: The outage probability versus *SNR* and different values of d.

loss of the users becomes larger.
The exact outage probability curves also match precisely with the Monte Carlo simulation results.

6. Conclusion

The DF relay based PSR and TSR protocols with DTT and DLT modes for EH and IP in wireless cooperative relaying networks have been studied in this paper. The close-form expressions of the outage probability, throughput, ergodic rate and EE for two users have derived. Furthermore, the expressions of the achievable throughtput, ergodic sum rate and EE for the users of the PSR and TSR protocols for SWIPT have also obtained. Based on our analytic as well as simulation results, it has shown that the CRNOMA outperforms the EE performance as compared to the conventional OMA. Also, the performance for the TSR protocol is superior to that for the PSR protocol in the common *SNR* region.

Conflicts of Interest

Authors declare there is no conflict of interest in this manuscript. This study was self-funded by the authors.

Appendices

6.1. Appendix A - Proofs of Theorem 1 and Theorem 5

From (21), the outage probability at R can be calculated by

$$\begin{aligned} P_{R,X} &= 1 - Pr\left(\frac{\psi_I^X |h_1|^2 a_2 \rho}{\psi_I^X |h_1|^2 a_1 \rho + 1} > \gamma_{th_2},\ \psi_I^X |h_1|^2 a_1 \rho > \gamma_{th_1}\right) \\ &= 1 - Pr(|h_1|^2 \geq \theta_{1,X}) \\ &= 1 - \int_{\theta_{1,X}}^{\infty} f_{|h_1|^2}(x) dx \end{aligned} \tag{47}$$

Applying (1), Eq. (47) can be obtained as follows

$$\begin{aligned} P_{R,X} &= 1 - \int_{\theta_{1,X}}^{\infty} \frac{1}{\Omega_1} e^{\frac{-x}{\Omega_1}} dx \\ &= 1 - e^{-\frac{\theta_{1,X}}{\Omega_1}} \end{aligned} \tag{48}$$

The proof is completed.

6.2. Appendix B - Proofs of Theorem 2 and Theorem 6

From (25), the expression can be obtained as follows

$$\begin{aligned} P_{D,X} = &\underbrace{P_r\left(|h_1|^2 < \tau_{1,X}\right)}_{J_2} + \\ &\underbrace{P_r\left(|h_1|^2 > \tau_{1,X}, |h_2|^2 < \frac{2\gamma_{th_2}}{|h_1|^2 \psi_E^X \rho}\right)}_{J_3} \end{aligned} \tag{49}$$

where J_2 can be determined by

$$J_2 = \int_0^{\tau_{1,X}} f_{|h_1|^2}(x)\, dx = 1 - e^{-\frac{\tau_{1,X}}{\Omega_1}} \tag{50}$$

The calculation process of J_3 is presented as

$$J_3 = \Pr\left(\tfrac{1}{2}|h_2|^2|h_1|^2\psi_E\rho < \gamma_{th_2}, \tfrac{|h_1|^2\psi_I a_2\rho}{\psi_I|h_1|^2 a_1\rho+1} > \gamma_{th_2}\right)$$

$$= \begin{cases} \Pr\left(|h_2|^2 < \frac{2\gamma_{th_2}}{|h_1|^2\psi_E\rho}, |h_1|^2 > \frac{\gamma_{th_2}}{\psi_I\rho\left(a_2-a_1\gamma_{th_2}\right)}\right), a_2 > a_1\gamma_{th_2} \\ 0,\ a_2 \le a_1\gamma_{th_2} \end{cases}$$

$$J_3 = \int_{\frac{\gamma_{th_2}}{\psi_I\rho\left(a_2-a_1\gamma_{th_2}\right)}}^{\infty} \int_0^{\frac{2\gamma_{th_2}}{x\psi_E\rho}} f_{|h_1|^2}(x) f_{|h_2|^2}(y)dxdy = \int_{\tau_1}^{\infty} \frac{1}{\Omega_1}\left[1-\exp\left(\frac{-2\gamma_{th_2}}{x\psi_E\rho\Omega_2}\right)\right]\exp\left(\frac{-x}{\Omega_1}\right)dx. \tag{51}$$

By substituting (50) and (51) into (49), the theorem is proved.

6.3. Appendix C - Proofs of Theorem 3 and Theorem 7

Firstly, the proof of (28) and (40) is presented in this appendix. To obtain this closed-form expression, the ergodic rate at R for CRNOMA can be written as

$$\begin{aligned} R_R^X &= \tfrac{1}{2}\mathrm{E}\left[\log_2\left(1+\psi_I^X|h_1|^2 a_1\rho\right)\right] \\ &= \tfrac{1}{2\ln 2}\int_0^{\infty}\tfrac{1-F_Y(x)}{1+x}dx \end{aligned} \tag{52}$$

The cumulative distribution function (CDF) of Y is calculated as follows

$$\begin{aligned} F_Y(x) &= \Pr\left(|h_1|^2 < \tfrac{x}{\psi_I^X a_1\rho}\right) \\ &= \int_0^{\frac{x(z\rho+1)}{\psi_I^X a_1\rho}} \tfrac{1}{\Omega_1}e^{-\frac{y}{\Omega_1}}dy \\ &= 1-e^{-\frac{x}{\psi_I^X a_1\rho\Omega_1}} \end{aligned} \tag{53}$$

By replacing (53) in (52), the ergodic rate at R can be derived as

$$R_R^X = \tfrac{1}{2}\tfrac{1}{\ln 2}\int_0^{\infty}\tfrac{1}{1+x}e^{-\frac{x}{\psi_I^X a_1\rho\Omega_1}}dx = \frac{-\exp\left(\frac{1}{\psi_I^X a_1\rho\Omega_1}\right)}{2\ln 2}Ei\left(\frac{-1}{\psi_I^X a_1\rho\Omega_1}\right) \tag{54}$$

The formulas of (28) and (40) can be derived. The proof is completed.

6.4. Appendix D - Proofs of Theorem 4 and Theorem 8

In this appendix, the proof begins by giving the ergodic rate at D as follows

$$R_D^X = E\left[\frac{1}{2}\log_2\left(1+\underbrace{\min\left(\gamma_{2,R},\gamma_{2,D}\right)}_{J_1}\right)\right]$$

$$J_1 = \underbrace{\min\left(\frac{\psi_I^X|h_1|^2 a_2\rho}{\psi_I^X|h_1|^2 a_1\rho+1}, |h_2|^2|h_1|^2\psi_E^X\rho\right)}_{Y}$$

The CDF of Y is calculated as follows by

$$F_Y(x) = \underbrace{\Pr\left(\frac{\psi_I^X|h_1|^2 a_2\rho}{\psi_I^X|h_1|^2 a_1\rho+1} < \frac{1}{2}|h_2|^2|h_1|^2\psi_E^X\rho, \frac{\psi_I^X|h_1|^2 a_2\rho}{\psi_I^X|h_1|^2 a_1\rho+1} < x\right)}_{I_3} +$$

$$\underbrace{\Pr\left(\frac{\psi_I^X|h_1|^2 a_2\rho}{\psi_I^X|h_1|^2 a_1\rho+1} > \frac{1}{2}|h_2|^2|h_1|^2\psi_E^X\rho, \frac{1}{2}|h_2|^2|h_1|^2\psi_E^X\rho < x\right)}_{I_4} \tag{55}$$

I_3 and I_4 are given by

$$\begin{aligned}
I_3 &= Pr\left(\frac{2\psi_I^X a_2}{\left(\psi_I^X|h_1|^2 a_1\rho+1\right)\psi_E^X} < |h_2|^2, |h_1|^2 < \frac{x}{\psi_I^X\rho(a_2-xa_1)}, \frac{a_2}{a_1}-x>0\right) \\
&= U\left(\frac{a_2}{a_1}-x\right)\times\int_0^{\frac{x}{\psi_I^X\rho(a_2-a_1x)}}\int_{\frac{2\psi_I^X a_2}{\left(\psi_I^X y a_1\rho+1\right)\psi_E^X}}^{\infty} f_{|h_1|^2}(y) f_{|h_2|^2}(z)\, dydz \\
&= U\left(\frac{a_2}{a_1}-x\right)\int_0^{\frac{x}{\psi_I^X\rho(a_2-a_1x)}}\exp\left(\frac{-2\psi_I^X a_2}{\left(\psi_I^X y a_1\rho+1\right)\psi_E^X\Omega_2}\right)\frac{1}{\Omega_1}\exp\left(\frac{-y}{\Omega_1}\right)dy \\
&= U\left(\frac{a_2}{a_1}-x\right)\int_0^{\frac{x}{\psi_I^X\rho(a_2-a_1x)}}\frac{1}{\Omega_1}e^{-\frac{2\psi_I^X a_2}{\left(\psi_I^X y a_1\rho+1\right)\psi_E^X\Omega_2}-\frac{y}{\Omega_1}}dy
\end{aligned} \tag{56}$$

$$
\begin{aligned}
I_4 &= \Pr\left(\frac{|h_1|^2\psi_I^X a_2\rho}{\psi_I^X|h_1|^2 a_1\rho+1} > \tfrac{1}{2}|h_2|^2|h_1|^2\psi_E^X\rho, \tfrac{1}{2}|h_2|^2|h_1|^2\psi_E^X\rho < x\right) \\
&= \Pr\left(|h_2|^2 < \tfrac{2\psi_I^X a_2}{\left(\psi_I^X|h_1|^2 a_1\rho+1\right)\psi_E^X}, |h_2|^2 < \tfrac{2x}{|h_1|^2\psi_E^X\rho}, \tfrac{a_2}{a_1}-x>0\right) \\
&= U\left(\tfrac{a_2}{a_1}-x\right)\Pr\left(|h_2|^2 < \tfrac{2\psi_I^X a_2}{\left(\psi_I^X|h_1|^2 a_1\rho+1\right)\psi_E^X}, |h_2|^2 < \tfrac{2x}{|h_1|^2\psi_E^X\rho}\right) \\
&= U\left(\tfrac{a_2}{a_1}-x\right)\times\Bigg[\underbrace{\Pr\left(|h_1|^2 < \frac{x}{\psi_I^X\rho\left(a_2-a_1x\right)}, |h_2|^2 < \frac{2\psi_I^X a_2}{\left(\psi_I^X|h_1|^2 a_1\rho+1\right)\psi_E^X}\right)}_{I_{41}}+ \\
&\qquad \underbrace{\Pr\left(|h_1|^2 > \frac{x}{\psi_I^X\rho\left(a_2-a_1x\right)}, |h_2|^2 < \frac{2x}{|h_1|^2\psi_E^X\rho}\right)}_{I_{42}}\Bigg]
\end{aligned}
\tag{57}
$$

I_{41} and I_{42} are calculated as follows

$$
\begin{aligned}
I_{41} &= \int_0^\infty \int_0^{\frac{x}{\psi_I^X\rho(a_2-a_1x)}} \int_0^{\frac{2\psi_I^X a_2}{\left(\psi_I^X y a_1\rho+1\right)\psi_E^X}} f_{|h_1|^2}(y) f_{|h_2|^2}(z)\, dydz \\
&= \int_0^{\frac{x}{\psi_I^X\rho(a_2-a_1x)}} \frac{1}{\Omega_1}\left(1-e^{-\frac{2\psi_I^X a_2}{\left(\psi_I^X y a_1\rho+1\right)\psi_E^X\Omega_2}}\right) e^{-\frac{y}{\Omega_1}} dy
\end{aligned}
\tag{58}
$$

And

$$
\begin{aligned}
I_{42} &= \int_{\frac{x}{\psi_I^X\rho(a_2-a_1x)}}^\infty \int_0^{\frac{2x}{y\psi_E^X\rho}} f_{|h_1|^2}(y) f_{|h_2|^2}(z)\, dydz \\
&= \int_{\frac{x}{\psi_I^X\rho(a_2-a_1x)}}^\infty \frac{1}{\Omega_1}\left(1-e^{-\frac{2x}{y\rho\psi_E^X\Omega_2}-\frac{y}{\Omega_1}}\right) dy
\end{aligned}
\tag{59}
$$

where $U(x)$ is unit step function as

$$U(x) = \begin{cases} 1, & x > 0 \\ 0, & x < 0 \end{cases}$$

From (58) and (59), (57) can be obtained. Substituting (57) and (56) into (55), the CDF of Y is given by

$$\begin{aligned} F_Y(x) = U\left(\frac{a_2}{a_1} - x\right) \Bigg[1 - e^{-\frac{x}{\psi_I^X \rho (a_2 - a_1 x)\Omega_1}} + \\ \int_{\frac{x}{\psi_I^X \rho (a_2 - a_1 x)}}^{\infty} \frac{1}{\Omega_1} \left(1 - e^{-\frac{2x}{y\rho \psi_E^X \Omega_2}}\right) e^{-\frac{y}{\Omega_1}} dy \Bigg] \end{aligned} \tag{60}$$

By replacing (60) in (29) and (41), the expressions of (30) and (42) can be obtained.
The proof is completed.

6.5. Appendix E - Proofs of Remark 1 and Remark 2

The proof begins by giving the ergodic rate at D for the high region as follows

$$\begin{aligned} R_{D,X}^{\infty} = E\left[\tfrac{1}{2}\log\left(1 + \min\left(\gamma_{2,R}, \gamma_{2,D}\right)\right)\right] = \frac{1}{2\ln 2} \int_0^{\infty} \frac{1 - F_Y(x)}{1+x} dx \\ I_5 = \underbrace{\min\left(\frac{a_2}{a_1}, \frac{1}{2}|h_2|^2 |h_1|^2 \psi_E^X \rho\right)}_{Y} \end{aligned} \tag{61}$$

The CDF of Y is calculated as follows

$$\begin{aligned}
F_Y(x) &= \Pr\left(\tfrac{a_2}{a_1} < \tfrac{1}{2}|h_2|^2|h_1|^2\psi_E^X\rho, \tfrac{a_2}{a_1} < x\right) + \\
&\quad \Pr\left(\tfrac{a_2}{a_1} > \tfrac{1}{2}|h_2|^2|h_1|^2\psi_E^X\rho, \tfrac{1}{2}|h_2|^2|h_1|^2\psi_E^X\rho < y, \tfrac{a_2}{a_1} > x\right) \\
&= \Pr\left(\tfrac{a_2}{a_1} > \tfrac{1}{2}|h_2|^2|h_1|^2\psi_E^X\rho, \tfrac{1}{2}|h_2|^2|h_1|^2\psi_E^X\rho < y, \tfrac{a_2}{a_1} > x\right) \\
&= U\left(\tfrac{a_2}{a_1} - x\right)\Pr\left(|h_1|^2 < \tfrac{2x}{\psi_E^X\rho|h_2|^2}, |h_1|^2 < \tfrac{2a_2}{a_1\psi_E^X\rho|h_2|^2}\right) \\
&= U\left(\tfrac{a_2}{a_1} - x\right)\Pr\left(\tfrac{a_2}{a_1} > x, |h_1|^2 < \tfrac{2x}{\psi_E^X\rho|h_2|^2}\right) + \\
&\quad U\left(\tfrac{a_2}{a_1} - x\right)\Pr\left(\tfrac{a_2}{a_1} < x, |h_1|^2 < \tfrac{2a_2}{a_1\psi_E^X\rho|h_2|^2}\right) \\
&= U\left(\tfrac{a_2}{a_1} - x\right)\Pr\left(\tfrac{a_2}{a_1} > x, |h_1|^2 < \tfrac{2x}{\psi_E^X\rho|h_2|^2}\right) \\
&= U\left(\tfrac{a_2}{a_1} - x\right)\int_0^\infty \int_0^{\frac{2x}{\psi_E^X\rho y}} f_{|h_2|^2}(y) f_{|h_1|^2}(z)\, dydz \\
&= U\left(\tfrac{a_2}{a_1} - x\right)\int_0^\infty \tfrac{1}{\Omega_2}\left(1 - e^{-\frac{2x}{\psi_E^X\rho\Omega_1 y}}\right) e^{-\frac{y}{\Omega_2}} dy \\
&= U\left(\tfrac{a_2}{a_1} - x\right)\left(1 - 2\sqrt{\tfrac{2x}{\psi_E^X\rho\,\Omega_1\Omega_2}}\, K_1\left(2\sqrt{\tfrac{2x}{\psi_E^X\rho\,\Omega_1\Omega_2}}\right)\right)
\end{aligned} \tag{62}$$

where $U(x)$ is unit step function as

$$U(x) = \begin{cases} 1, & x > 0 \\ 0, & x < 0 \end{cases}$$

Substituting (62) into (61), the expression of $R_{D,X}^{\infty}$ can be obtained. The proof is completed.

Reference

[1] Dai, L., Wang, B., Ding, Z., Wang, Z., Chen, S. and Hanzo, L.,.: A survey of non-orthogonal multiple access for 5G, IEEE Communications Surveys & Tutorials, 2018, 20, (3), pp.2294-2323.

[2] Ding, Z., Lei, X., Karagiannidis, G.K., Schober, R., Yuan, J. and Bhargava, V.K.,.: A survey on non-orthogonal multiple access for 5G networks: Research challenges and future trends, IEEE Journal on Selected Areas in Communications, 2017, 35, (10), pp.2181-2195.

[3] Islam, S.M., Zeng, M. and Dobre, O.A., .: NOMA in 5G systems: Exciting possibilities for enhancing spectral efficiency, arXiv preprint arXiv:1706.08215, 2017.

[4] Wei, Z., Yuan, J., Ng, D.W.K., Elkashlan, M. and Ding, Z., .: A survey of downlink non-orthogonal multiple access for 5G wireless communication networks, arXiv preprint arXiv:1609.01856, 2016.

[5] H. Q. Tran, P. Q. Truong, C. V. Phan, and Q.-T. Vien.: On the energy efficiency of NOMA for wireless backhaul in multi-tier heterogeneous CRAN, in Proc. SigTelCom, Da Nang, Vietnam, January 2017, pp. 229-234.

[6] Q.-T. Vien, T. A. Le, C. V. Phan, and M. O. Agyeman.: An energy-efficient NOMA for small cells in heterogeneous CRAN under QoS constraints, in Proceedings European Wireless Conference (EW 2017), Dresden, Germany, May 2017, pp. 80-85.

[7] Q.-T. Vien, T. A. Le, B. Barn and C. V. Phan.: Optimising energy efficiency of non-orthogonal multiple access for wireless backhaul in heterogeneous cloud radio access network, IET Communications, 2016, 10, (18), pp. 2516-2524.

[8] N. Bhuvanasundaram, H. X. Nguyen, R. Trestian, and Q.-T. Vien.: Non-orthogonal multiple access schemes for next-generation 5G networks: A survey. In: 5G Radio Access Networks: Centralized RAN, Cloud-RAN and Virtualization of Small Cells, CRC Press, 2017, pp. 51-66.

[9] H. Q. Tran, C. V. Phan, and Q.-T. Vien.: An overview of 5G technologies. In: EmergingWirelessCommunication & NetworkTechnologies:Principle,Paradigm and Performance, Springer, 2018, pp. 59-80.

[10] X.Su, A. Castiglione, C. Esposito, C. Choi, Power domain NOMA to support group communication in public safety networks, Future Generation Computer Systems, Jul. 2018, vol. 84, pp. 228-238.

[11] S.M. R. Islam, N. Avazov, O. A. Dobre, K. S. Kwak, Power-Domain Non-Orthogonal Multiple Access (NOMA) in 5G Systems: Potentials and Challenges, IEEE Communications Surveys & Tutorials, Oct. 2016, Vol. 19, pp. 721 - 742.

[12] O. Shental, B. M. Zaidel, S. S. Shitz, Low-density code-domain NOMA: Better be regular, IEEE International Symposium on Information Theory (ISIT), Aug. 2017.

[13] Ding, Z., Fan, P. and Poor, H.V., , Impact of user pairing on 5G nonorthogonal multiple-access downlink transmissions, IEEE Transactions on Vehicular Technology, 2016, 65 (8), pp.6010-6023.

[14] Sun, Y., Ng, D.W.K., Ding, Z. and Schober, R., Optimal joint power and subcarrier allocation for full-duplex multicarrier non-orthogonal multiple access systems, IEEE Transactions on Communications, 2017, 65, (3), pp.1077-1091.

[15] Y. Zhang, Z. Yang, Y. Feng, S. Yan, Performance Analysis of Cooperative Relaying Systems with Power-Domain Non-Orthogonal Multiple Access, IEEE Access, Jul. 2018, vol. 6, pp. 2169-3536.

[16] Islam, S. R., Avazov, N., Dobre, O. A., & Kwak, K. S, Power-domain non-orthogonal multiple access (NOMA) in 5G systems: Potentials and challenges, IEEE Communications Surveys & Tutorials, 2016, 19(2), pp.721-742.

[17] Sadia, H., Zeeshan, M., & Sheikh, S. A, Performance analysis of downlink power domain NOMA under fading channels, IEEE, In 2018 ELEKTRO, pp. 1-6.

[18] H. Q. Tran, C. V. Phan, and Q.-T. Vien, On the performance of regenerative relaying for SWIPT in NOMA Systems, 26th International Conference on Telecommunications (ICT 2019), Apr.2019, (Accepted/In press).

[19] D. Wang, Y. Li, Y. Ye et al., Joint time allocation and power splitting schemes for df energy harvesting relaying networks, in Proc. IEEE 86nd Vehicular Tech. Conf., 2017, to appear, pp. 15.

[20] C. K. Ho and R. Zhang, Optimal energy allocation for wireless communications with energy harvesting constraints, IEEE Trans. Signal Process., 2012, vol. 60, no. 9, pp. 48084818.

[21] Y. Ye, Y. Li, D. Wang, G. Lu, Power splitting protocol design for the cooperative NOMA with SWIPT, IEEE International Conference on Communications (ICC), 2017, pp. 1-5).

[22] A. Rauniyar, P. Engelstad, O. N. Osterbo, RF Energy Harvesting and Information Transmission Based on NOMA for Wireless Powered IoT Relay Systems, Sensors, Sep. 2018, vol. 18, no. 10, 3254.

[23] Y. Wang, Y. Wu, F. Zhou, Z. Chu, , Y. Wu, F. Yuan, Multi-Objective Resource Allocation in a NOMA Cognitive Radio Network With a Practical Non-Linear Energy Harvesting Model, IEEE Access, Dec. 2017, vol. 6, pp. 12973 - 12982.

[24] S. Ulukus, A. Yener, E. Erkip, O. Simeone, M. Zorzi, P. Grover, K. Huang, Energy harvesting wireless communications: a review of recent advances, IEEE Journal on Selected Areas in Communications, Jan. 2015, vol. 33, pp. 360381.

[25] D. B. Ha, S. Q. Nguyen, Outage Performance of Energy Harvesting DF Relaying NOMA Networks, Mobile Networks and Applications, Dec. 2018, vol. 23, pp. 15721585.

[26] A. A. Nasir, X. Zhou, S. Durrani, and R. A. Kennedy, Relaying protocols for wireless energy harvesting and information processing, IEEE Trans. Wireless Commun., 2013, vol. 12, no. 7, pp. 36223636.

[27] M. Ju,K. M. Kang, K. S. Hwang, C. Jeong, Maximum transmission rate of PSR/TSR protocols in wireless energy harvesting DF-based relay networks, IEEE Journal on Selected Areas in Communications, 2015, vol. 33 (12), pp. 2701-2717.

[28] Y. Gu and S. Assa, RF-based energy harvesting in decode-and-forward relaying systems: Ergodic and outage capacities, IEEE Trans. Wireless Commun., 2015, vol. 14, no. 11, pp. 64256434.

[29] Xu, Y., Shen, C., Ding, Z., Sun, X., Yan, S., Zhu, G., and Zhong, Z., Joint beamforming and power-splitting control in downlink cooperative SWIPT NOMA systems, IEEE Transactions on Signal Processing, 2017, 65 (18), pp. 4874-4886.

[30] Ly, T.T.H., Nguyen, H.S., Nguyen, T.S., Huynh, V.V., Nguyen, T.L. and Voznak, M., Outage probability analysis in relaying cooperative systems with NOMA considering power splitting, Symmetry, 2019, vol. 11, no. 1, p.72.

[31] Ye, Y., Li, Y., Wang, D., Lu, G. , Power splitting protocol design for the cooperative NOMA with SWIPT, IEEE International Conference on Communications (ICC), 2017, pp. 1-5.

[32] Liu, Y., Ding, Z., Eikashlan, M., Poor, H. V. , Cooperative non-orthogonal multiple access in 5G systems with SWIPT, European signal processing conference (EUSIPCO), 2015, pp. 1999-2003.

[33] X. Yue, Y. Liu, S. Kang, A. Nallanathan, Z. Ding, Exploiting full/half-duplex user relaying in NOMA systems, IEEE Transactions on Communications, 2017, vol. 66, no.2, pp. 560-575.

[34] Liau, Qian Yu, and Chee Yen Leow, Analysis of opportunistic two-path successive relaying in consideration of inter-relay interference, IET Communications 11, no. 1 (2017): 76-84.

[35] Luo, Chunbo, Yu Gong, and Fuchun Zheng, Full interference cancellation for two-path relay cooperative networks, IEEE Transactions on Vehicular Technology 60, no. 1 (2010): 343-347.

[36] Liau, Qian Yu, Chee Yen Leow, and Zhiguo Ding, Amplify-and-forward virtual full-duplex relaying-based cooperative NOMA, IEEE Wireless Communications Letters 7, no. 3 (2017): 464-467.

[37] K., Md Fazlul, M. B. Uddin, A. Islam, S. Y. Shin, Cooperative non-orthogonal multiple access with SWIPT over Nakagami−m fading channels, Transactions on Emerging Telecommunications Technologies, 2019, no. 5.

[38] J., Neha, V. A. Bohara, Energy harvesting and spectrum sharing protocol for wireless sensor networks, IEEE Wireless Communications Letters, 2015,vol. 4, no. 6, pp. 697-700.

[39] A. Amin, Ahmed, S. Y. Shin, Investigate the Dominating Factor of Hybrid SWIPT Protocol by Performance Analysis of the Far User of Hybrid SWIPT based CNOMA Downlink Transmission, In 2019 International Conference on Electrical, Computer and Communication Engineering (ECCE), 2019, pp. 1-6.

[40] Son, P.N., Kong, H.Y. & Anpalagan, A, Exact outage analysis of a decode-and-forward cooperative communication network with N th best energy harvesting relay selection, Ann. Telecommun. 71, pp. 251263 (2016).

[41] Y. Wang, B. Ren, S. Sun, S. Kang, and X. Yue, Analysis of Non-Orthogonal Multiple Access for 5G, China Commun., 2016, vol. 13, no.Supplement No. 2, pp. 52-66.

[42] S. Luo, R. Zhang, and T. J. Lim, Optimal save-then-transmit protocol for energy harvesting wireless transmitters, Transactions on Wireless Communications, 2013, vol.13, no.3, pp. 1196-1207.

[43] Gradshteyn, I.S., Ryzhik, I.M, "Table of integrals, series and products," *Academic, San Diego, CA*, 7th edn, 2007.

Tran Quy Huu received the M.S degree in Electronics Engineering from Ho Chi Minh City University of Technology and Education (HCMUTE), Viet Nam, in 2010. Currently, he has been working as a lecturer at Faculty of Electronics Technology, Industrial University of Ho Chi Minh City (IUH), Viet Nam. He is also a PhD candidate at Faculty of Electrical - Electronics Engineering, Ho Chi Minh City University of Technology and Education, Viet Nam. His research interests include Wireless Communications, Non-orthogonal Multiple Access (NOMA), Energy Harvesting (EH), Wireless Cooperative Relaying Networks, Heterogeneous Networks (HetNet), and Cloud Radio Access Networks (C-RAN).

Phan Van Ca received the PhD degree in Electronics and Radio Engineering from Kyung Hee University, Republic of Korea, in 2010. He is currently an Associate Professor at the Department of Computer and Communications Engineering, Faculty of Electrical and Electronics Engineering, Ho Chi Minh City University of Technology and Education, Viet Nam. His main research interests include wireless networks and mobile systems design and performance evaluation, dynamic programming techniques, Markov decision process, ubiquitous computing and embedded systems, and internet of things.

Quoc-Tuan Vien (S'10, M'12, SM'15) received his Ph.D. degree in Telecommunications from Glasgow Caledonian University, U.K., in 2012. He is currently a Senior Lecturer with the Faculty of Science and Technology at Middlesex University, U.K. He has authored a textbook, co-authored five book chapters, and over 80 publications in ISI journals and major conference proceedings. His current research interests include physical-layer security, network coding, non-orthogonal multiple access, R-F energy harvesting, device-to-device communications, heterogeneous networks, and Internet of Things. He currently serves as an Editor of the INTERNATIONAL JOURNAL OF DIGITAL MULTIMEDIA BROADCASTING, a Guest Editor of the EAI ENDORSED TRANSACTIONS ON INDUSTRIAL NETWORKS AND INTELLIGENT SYSTEMS, a Program Co-Chair for the EAI International Conference on Industrial Networks and Intelligent Systems (INISCOM 2018, 2019), and a Technical Symposium Co-Chair for the International Conference on Recent Advances in Signal Processing, Telecommunications and Computing (SigTelCom 2017-2019). He was a recipient of the Best Paper Award at the IEEE/IFIP 14th International Conference on Embedded and Ubiquitous Computing in 2016. He was honored as an Exemplary Reviewer of the IEEE COMMUNICATIONS LETTERS in 2017.